





Article

# Analysis of Mixed Traffic Flow Characteristics Based on Fleet Composition

Huanfeng Liu <sup>1,2</sup> , Keke Niu <sup>1,2</sup>, Hanfei Wang <sup>1,2,\*</sup> , Ziyan Wu <sup>1,2</sup>  and Anning Song <sup>1,2</sup> 

<sup>1</sup> School of Traffic and Transportation, Shijiazhuang Tiedao University, Shijiazhuang 050043, China; huanfengliu@stdu.edu.cn (H.L.); 1202106080@student.stdu.edu.cn (K.N.); 1202306026@student.stdu.edu.cn (Z.W.); 1202306054@student.stdu.edu.cn (A.S.)

<sup>2</sup> Hebei Key Laboratory of Traffic Safety and Control, Shijiazhuang 050043, China

\* Correspondence: 1202206094@student.stdu.edu.cn; Tel.: +86-15382117680

**Abstract:** In urban road networks, the integration of connected and autonomous vehicles (CAV) significantly influences traffic flow patterns, with the Fleet Composition—representing the positioning of these vehicles within convoys—being crucial in dictating the symmetry of information exchange amongst them. First, the vehicle composition of the mixed traffic flow is analyzed, and the mathematical analytical expressions of the random distribution characteristics of different types of vehicles are constructed. Second, we analyze the vehicle according to human characteristics in different situations. Then, consider the following characteristics and reaction times of manual drivers, establish a mixed traffic flow following model, and validate the established following. Finally, the basic graph model considering Fleet Composition is derived, and the effects of reaction time, Fleet Composition, driver following characteristics, and other parameters on road capacity under different penetration rates of CAV are analyzed by a Python and SUMO joint simulation. Finally, the characteristics of mixed traffic flow at intersections were analyzed.

**Keywords:** mixed traffic flow; fleet composition; symmetry in information exchange; vehicle following characteristics; CAV penetration rate



**Citation:** Liu, H.; Niu, K.; Wang, H.; Wu, Z.; Song, A. Analysis of Mixed Traffic Flow Characteristics Based on Fleet Composition. *Symmetry* **2024**, *16*, 865. <https://doi.org/10.3390/sym16070865>

Academic Editors: Guangdong Tian, Yong Peng, Zhiwu Li, Amir M. Fathollahi-Fard and Honghao Zhang

Received: 13 May 2024

Revised: 24 June 2024

Accepted: 24 June 2024

Published: 8 July 2024



**Copyright:** © 2024 by the authors. Licensee MDPI, Basel, Switzerland. This article is an open access article distributed under the terms and conditions of the Creative Commons Attribution (CC BY) license (<https://creativecommons.org/licenses/by/4.0/>).

## 1. Introduction

With the unsustainable expansion of transportation infrastructure, such as road resources, the solution to the traffic congestion problem has become dependent on traffic control measures. Existing control measures for vehicle guidance must work through the human driver, and the relationship between the two is loosely coupled. In the perception and control process of human drivers, there is a large amount of uncertainty and differentiation in the degree of obedience factors, resulting in a certain number of random disturbances and behavioral differences in the actual driving process of the vehicle, resulting in a decline in the efficiency of the control measures.

The emergence of intelligent networked vehicles (connected and autonomous vehicles, CAV) provides a new way of thinking to solve existing traffic problems. CAV has solved the problem from loose coupling to tight coupling between the control methods and the human drivers due to their network connectivity and driverless characteristics. However, the development of technology is not overnight; before the complete realization of all the intelligent network connections, the phenomenon of CAV and traditional artificial driving vehicles (Human-Driven Vehicles, HDV) will become the norm.

With the advent of CAV, the existing traffic environment has become more complex. Not only do we have to consider the synergistic problems of HDV, vehicle-road, vehicle-vehicle, vehicle-infrastructure, etc., but also the influence of factors such as human drivers' attitudes toward CAV and the ever-changing penetration rate of CAV. The penetration rate of CAV in a traffic flow refers to the penetration rate of CAVs within the traffic stream. This metric reflects the distribution of CAVs throughout the entire traffic flow, measuring their

degree of penetration in the mixed traffic environment. Therefore, traditional traffic flow models and traffic control measures will no longer be applicable to the new traffic environment, and many scholars have conducted prospective studies to grasp the characteristics of the new mixed traffic flow.

In terms of mixed traffic flow sequential modeling, many scholars have used different sequential models as sequential models for different situations in mixed traffic flow, such as the CTH and MCD cellular automata models [1], the IDM model [2,3], the CACC model [4], and so on. Furthermore, Ziyu Cui et al. [5] extended the IDM model to include multiple vehicles' positions, velocities, and accelerations, adapting it to the characteristics of heterogeneous traffic. There are also scholars who improve the Gipps model [6,7]. In addition, Xinjuan Ma [8] et al. improved the vehicle following the model based on OVM (Optimal Velocity Model) by using the driver's memory. Zong Fang [9] et al. considered the characteristics of multiple front vehicles based on the full speed difference model and concluded that the time for the convoy to recover stability decreases with the increase in the penetration rate of CAV.

Regarding the characteristics of mixed traffic flow, Qin Yanyan [10] et al. utilized the basic diagram model of traffic flow, established a general analytical framework, and used the LWR model to describe the propagation of shock waves in mixed traffic flow. Subsequently, very many scholars have used the basic graph model to analyze the impact of different penetration rates of CAV [11–13] on the road capacity. Some other scholars have also focused their research on the energy saving and emission reduction [13–16] contribution of CAV to energy saving and emission reduction. In addition, Ye [17] et al. focus on the safety of mixed traffic flow, establish a mixed traffic flow model under the state of CAV, and analyze the effects of acceleration, speed, and penetration rate of CAV on driving safety, construct a basic graph model to describe mixed traffic flow and analyze the effects of different penetration rates of CAV on road capacity. Wang [18] et al. constructed a CTM traffic assignment model to describe mixed traffic flow and designed the RSRS-MARA algorithm to predict traffic congestion. Yang Xujian [19] et al. constructed a model to reflect the coupling relationship between the dynamic characteristics of vehicle queues and traffic flow and analyzed the impact of penetration rate on accessibility. Dehua Wu [20] et al. introduced relative entropy as a parameter describing the characteristics of heterogeneous traffic flow and used the improved NaSch model to simulate the degree of CAV.

In summary, most of the scholars consider different following characteristics in different situations when establishing the mixed traffic flow following model, but in the context of traffic flow, the behavioral characteristics of human drivers are also of paramount importance. Xiaoyun Chen [21] integrated human factors by examining both the long-term inherent driving patterns of drivers and their short-term changes in response to external stimuli, proposing a model that combines long- and short-term driving features (LSTD). Conversely, Shubham Soni [22] and others focused on analyzing the interaction between human drivers and autonomous vehicles (AVs), particularly the level of trust exhibited by human drivers towards AVs. Building upon these foundations, the current study further explores the impact of reaction time and psychological factors when human drivers follow connected and intelligent vehicles. It categorizes trust levels into hesitant, stable, and trusting types, thereby refining existing models and establishing a mixed traffic flow car-following model. Additionally, considering that the positional distribution of CAV within a platoon affects information exchange, this study uses fundamental diagram models to analyze the characteristics of potential future mixed traffic flows—such as variations in flow and density and the impact of various factors on road capacity—so planners can allocate road lanes more scientifically (for instance, by considering the implementation of dedicated lanes for CAV). This ensures that road infrastructure can adapt to potential future changes, thereby enhancing the overall efficiency of the road network. Finally, this study examines the performance of mixed traffic flow at signalized intersections under different penetration rates of CAV, providing a theoretical foundation for designing management systems aimed at reducing delays and improving traffic flow efficiency.

## 2. Mixed Traffic Composition

### 2.1. Vehicle Functional Degradation and Classification

There are two main ways for intelligent CAVs to optimize their driving state by obtaining traffic information: one is to use on-board equipment to detect the speed difference, distance, and other data information with the vehicle in front of them, and the other is to share information with the vehicle in front of them through vehicle-to-vehicle (V2V) wireless communication. The latter is more capable of obtaining relevant information in a timely and accurate manner compared to the former. If both neighboring vehicles are CAV, the rear vehicle can establish communication with the front vehicle through the vehicle-to-vehicle wireless communication function. At this time, the information interaction between the front and rear cars is symmetrical. However, this symmetry is often not necessarily equal. If the front vehicle is not a CAV, the rear vehicle cannot share information with it and cannot use the vehicle-to-vehicle wireless communication function, but it will use its own on-board equipment to obtain the information of the front vehicle in the first place and optimize its own driving state, which is referred to as the degraded function of CAV in this study, and the rear vehicle is referred to as a degraded intelligent networked vehicle (DCAV). A degraded CAV can still share information with the rear vehicle, which is also a DCAV, through its own vehicle-to-vehicle wireless communication function. Therefore, whether a DCAV is in a degraded state or not is determined by the traffic environment in which it is located.

For the future mixed traffic flow on urban roads where CAV and HDV coexist, the relative positions of the vehicles are randomly distributed, so the following four kinds of following situations will be formed (Figure 1), which are finally categorized into three kinds of situations: CAV following CAV (case1); CAV following HDV (case2); HDV following HDV (case3); and HDV following CAV (case4).

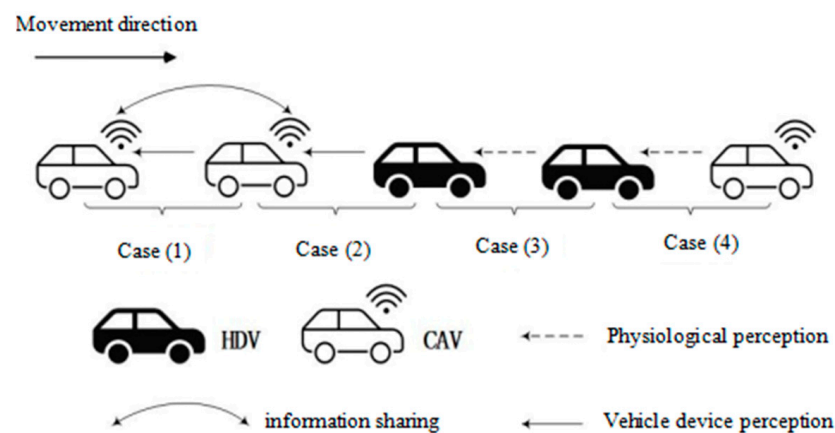


**Figure 1.** Vehicle following situation in mixed traffic flow (CAV: connected and autonomous vehicles; HDV: Human-Driven Vehicles).

### 2.2. Vehicle Scale Relationship Analysis Expression

#### (1) Impact of different follow-through scenarios

In this study, the numbers 1 and 0 are used to represent the CAV and HDV, respectively. Assuming that the penetration rate of CAV in the mixed traffic flow on urban roads is  $P_1$ , the penetration rate of HDV is  $P_0 = 1 - P_1$ , and there are  $N$  vehicles in the traffic flow, and from the level of probabilistic theory, the penetration rates of the vehicles corresponding to the four types of following scenarios summarized above are shown in Table 1:

**Table 1.** Percentage of vehicles in the following situations.

Follow the Herd 1	Follower Type	Rear Vehicle Type	Percentage of Vehicles	Number of Vehicles
1	CAV follows CAV	CAV	$P_1 \times P_1$	$NP_1^2$
2	CAV follows HDV	DCAV	$P_1 \times (1 - P_1)$	$NP_1P_0$
3	The rear vehicle is HDV	HDV	$(1 - P_1) \times (1 - P_1)$	$NP_0$
4			$(1 - P_1) \times P_1$	

(2) Impact of Fleet Composition

In the mixed traffic flow mixed with CAV, the Fleet Composition is used to reflect the distribution and agglomeration of CAV, which is denoted by the symbol  $O$  with the value range of  $[-1, 1]$ . In the case of a certain penetration rate of mixed CAV, the higher the Fleet Composition and the more concentrated the distribution of CAV, the higher the Fleet Composition, and thus a high degree of assembly occurs.

The situation when the CAV is 50% is shown in Figure 2.

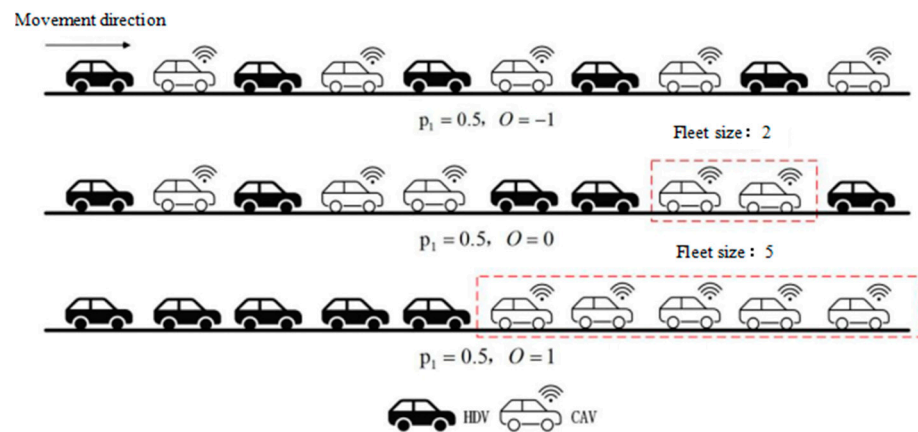


**Figure 2.** Schematic diagram of the fleet structure.

At this time, due to the formation of different Fleet Compositions, the CAV, DCAV, and HDV three types of vehicles accounted for a different penetration rate, that is, a certain penetration rate of CAV. The Fleet Composition was an independent variable, and at this time, all types of vehicles accounted for the dependent variable. Therefore, the Fleet Composition of the mixed traffic flow affected the probability of the occurrence of the different following models.

The probability of a CAV following HDV occurring when the penetration rate of CAV is  $P_1$  and the Fleet Composition of mixed traffic flow is  $O$  can be represented by  $P_{10} = (P, O)$ , then the different following scenarios are uniformly represented by  $P_{mn} = (P, O)$ , where  $m, n = 0, 1$ .

(3) Penetration rate of vehicles in the following situations

Abstracting the fleet as a Markov chain [23], the probability of occurrence of different following scenarios, the penetration rate of CAV  $P_1$  and the Fleet Composition of mixed traffic flow  $O$  are modeled as parameters according to (1) and (2), and the penetration rate of vehicles in different following scenarios is shown in the following equation.

$$P_{10}(P_1, O) = \begin{cases} P_0(1 - O), & 0 \geq O; \\ P_0 + O(P_0 - \min\{1, \frac{P_0}{P_1}\}), & 0 \leq O \end{cases} \quad (1)$$

$$P_{11}(P_1, O) = 1 - P_{10}(P_1, O) \quad (2)$$



$$P_{01}(P_1, O) = \begin{cases} P_1(1 - O), 0 \geq O; \\ P_1 + O(P_1 - \min\{1, \frac{P_1}{P_0}\}), 0 \leq O \end{cases} \quad (3)$$

$$P_{00}(P_1, O) = 1 - P_{01}(P_1, O) \quad (4)$$

In the actual mixed traffic flow on urban roads, there is no vehicle in front of the head car in the traffic flow, which cannot form the above-mentioned situation. When there are vehicles in the traffic flow, to ignore the influence of the head car space headway and the tail car length, this study is large enough to obtain the number of situations where the car model follows the car model. The number of situations where the model follows the model can be obtained for:

$$N_{mm} = NP_m P_{mn}(P_1, O) \quad (5)$$

### 3. Mixed Traffic Flow Car-Following Model

#### 3.1. Car-Following Modeling in Different Scenarios

According to the composition of the mixed traffic flow, there are differences in the interaction ability between different types of vehicles and the traffic environment, and the following behavior is different in different situations, so different following models are adopted to express their driving characteristics.

##### (1) CAV follows CAV.

The Cooperative Adaptive Cruise Control (CACC) model proposed by the PATH Lab at the University of California, Berkeley, is based on the constant inter-vehicle time-distance strategy [24]. It is a popular model used for the research of CAV, and its control method is based on vehicle-to-vehicle communication technology, which can sense the traffic environment in a more comprehensive, timely, and accurate way and can better express the driving characteristics of the CAV in this study.

After the calibration of the parameters in the PATH laboratory, the control distance error and its differential term are 0, to achieve the purpose of control with a constant desired workshop time distance, according to the results of the real vehicle experiments in the PATH laboratory [25]. According to the results of real vehicle experiments in the PATH laboratory, the values of the desired workshop time distance  $t_c$  are shown in Table 2.

**Table 2.** Values and acceptance ratio of desired workshop spacing  $t_c$ .

Time Headway $t_c/s$	Driver Acceptance Rate/%
0.6	57.0
0.7	24.0
0.9	7.0
1.1	12.0

To summarize, the CAV car-following model is presented using the CACC model with the following expression:

$$\begin{cases} v = v_{pre} + k_p e + k_d \dot{e}, \\ e = x_c - s_c - l - t_c v \end{cases} \quad (6)$$

where:  $v_{pre}$  is the speed at the previous instant.

$e$  is the difference between the actual shop distance and the desired shop distance.

$\dot{e}$  is the difference in the workshop distance error.

$x_c$  is the space headway of the CAV.

$l$  is the length of the vehicle, assumed to be 5 m;

$s_c$  is the minimum safety distance for CAV, which is taken as 2 m;

$t_c$  is the desired inter-vehicle time distance for CAV, taken as the highest value of the driver acceptance ratio of 0.6 s;

$v$  is the current speed.

$k_p$  and  $k_d$  are the control coefficients, with reference to the calibration results of the CACC model in real vehicle experiments,  $k_p$  and  $k_d$  are taken as 0.45 and 0.25, respectively.

Performing a first-order Taylor expansion of  $v$  in the CACC model expression yields the acceleration equation as follows:

$$a_c = \frac{k_p(x_c - s_c - l - k_d \Delta v)}{\Delta t + k_d t_c} \quad (7)$$

where:  $a_c$  is the acceleration of the CAV.

$\Delta v$  is the speed difference between two neighboring cars.

$\Delta t$  For the speed update interval, refer to the PATH real vehicle experiment to take 0.01 s.

(2) CAV follows HDV.

Adaptive Cruise Control (ACC) based on constant desired space headway is an improved IDM model obtained by changing the safe headway time distance in the IDM model, which can obtain information about the surrounding vehicle traveling through its own equipment and fits with the degraded DCAV characteristics of the CAV. According to the results of real-vehicle experiments in the PATH laboratory [24], the values of the desired headway time distance  $t_d$  are shown in Table 3.

**Table 3.** Values and acceptance ratio of desired workshop spacing  $t_d$ .

Time Headway $t_d/s$	Driver Acceptance Rate/%
0.6	57.0
1.1	50.4
1.6	18.5
2.2	31.1

When the CAV follows the HDV, rear vehicle degradation occurs, i.e., degradation from CACC to ACC. Therefore, when the front vehicle is an artificial driving vehicle and the rear vehicle is a CAV, the ACC model proposed by PATH Laboratory based on the constant time headway strategy is adopted, and its expression is as follows:

$$a_d = k_1(x_d - s_d - l - t_d v) + k_2 \Delta v \quad (8)$$

where:  $a_d$  is the acceleration of the degraded CAV.

$x_d$  is the space headway after the degradation of the CAV.

$s_d$  is the minimum safe distance after degradation of the CAV, taken as 2 m;

$t_d$  is the desired inter-vehicle time distance after degradation of the CAV, again taking the highest value of the driver acceptance ratio of 1.1 s;

$k_1$  and  $k_2$  are the control coefficients, and  $k_1$  and  $k_2$  are taken as  $0.23 \text{ s}^{-2}$  and  $0.07 \text{ s}^{-1}$ , respectively, with reference to the calibration results of the CACC model from the real vehicle experiments.

(3) HDV as Followers

The intelligent Driver Model (IDM) was proposed by German scholar Treiber [25] et al. The model has the advantages of a small number of parameters and clear physical meaning, which can better reflect the characteristics of the following of the HDV, so the IDM model is selected in this study to express the situation when the HDV is a following vehicle.

Urban roads are divided into two kinds: ordinary roads and expressways, and this paper studies the ordinary sections of urban roads. According to the Regulations of the People's Republic of China on the Implementation of the Road Traffic Safety Law [26], the speed limit of the ordinary section of the urban road is 40 km/h, i.e., 11 m/s.

When the following vehicle is an HDV, the IDM model is taken, and its expression is as follows:

$$a_h = a_{\max} \left\{ 1 - \left( \frac{v}{v_f} \right)^4 - \left[ \frac{s_h + vt_h + v\Delta v(2\sqrt{a_{\max}b})^{-1}}{x_h - l} \right]^2 \right\} \quad (9)$$

where:  $a_h$  is the acceleration of the HDV;

$a_{\max}$  is the maximum acceleration, taken as  $1 \text{ m/s}^2$ ;

$v_f$  is the free stream velocity, taken as  $11.1 \text{ m/s}$ ;

$s_h$  is the minimum safe distance for HDV, taken as  $2 \text{ m}$ ;

$t_h$  is the desired safe headway time distance for a HDV, taken as  $1.5 \text{ s}$ ;

$b$  is the desired comfortable deceleration for a HDV, taken as  $2.8 \text{ m/s}^2$ ;

$x_h$  is the space headway of an HDV.

### 3.2. Mixed Traffic Flow Following Model Based on Following Characteristics and Reaction Time

Although the above section has used different following models to express the following behavior in different situations, the actual situation is more complicated for mixed traffic flow. To be more in line with the real traffic environment, the driver's following characteristics and reaction time are introduced in the construction of the mixed traffic flow following model.

#### (1) Driver follower characteristics

When an HDV is used as a vehicle, the following behavior may be significantly different depending on the driver's style. Based on the degree of trust the human driver has with the CAV, the situation in which the human driver follows the CAV can be classified into the following three styles: hesitant, smooth, and trusting [27]. In this study, based on the calibration of the maximum acceleration and safe following distance for the three types of following styles, the maximum acceleration sensitivity coefficient  $\lambda_n$  and the safe headway distance sensitivity coefficient  $\omega_n$  are introduced, and the situation of the HDV following an HDV with a following style defined as normal, which is not affected by the two sensitivity coefficients, and the values of the two sensitivity coefficients are taken as 1, respectively, the expressions of the improved IDM model are obtained as follows:

$$a_h = \lambda_n a_{\max} \left\{ 1 - \left( \frac{v}{v_f} \right)^4 - \left[ \frac{s_h + v\omega_n t_h + v\Delta v(2\sqrt{a_{\max}b})^{-1}}{x_h - l} \right]^2 \right\} \quad (10)$$

where:  $n$  takes the values of 1, 2 and 3 to indicate the three types of following styles: hesitant, smooth, and trusting, respectively.

The values of the sensitivity factors  $\lambda_n$  and  $\omega_n$  are shown in Table 4:

**Table 4.** Values of the sensitivity coefficients  $\lambda_n$ ,  $\omega_n$  and the style of Car-following.

Driving Style	Maximum Acceleration Sensitivity Factor $\lambda_n$	Safe Headway Time Sensitivity Factor $\omega_n$
hesitant	0.97	1.91
stable	1.31	1.30
trust-based	1.70	0.65
normal type	1.00	1.00

#### (2) Reaction time

Reaction time refers to the reaction time of a vehicle in the face of a complex traffic environment, i.e., the time required for the driver's physiological perception process or the vehicle-vehicle transmission and reception of information. In the case of HDV, it includes the time required for reaction processes such as sensing, recognizing, and judging, while in the case of CAV, it refers to the delay perceived by the on-board system during vehicle-to-vehicle information transmission and reception.

Vehicles in the driving process are usually used to prevent sudden driving changes and maintain a certain safety distance from the front car  $t$ , to avoid traffic accidents. Therefore, the model should take into account the situation when the front vehicle suddenly undergoes a driving change. At this time, the rear vehicle cannot react immediately and still maintains the original driving state within the reaction time  $\tau$ , then the actual time used by the rear vehicle is  $t - \tau$ , which is smaller than the original safety time distance in the following model, so the headway is compensated for, and the headway after the compensation is  $t'$ , whose expression is as follows:

$$t' = t + \tau \quad (11)$$

In summary, the three types of models are improved by adding reaction time to the original minimum headway time distance  $\tau$ .

① CACC for CAV

The improved CACC Car-following model expression is as follows:

$$a_c = \frac{k_p(x_c - s_c - l - (t_c + \tau_c)v) + k_d\Delta v}{\Delta t + k_d t_c} \quad (12)$$

② Degraded DCAV for CAV

The improved expression for the ACC Car-following model is as follows:

$$a_d = k_l[x_d - s_d - l - (t_d + \tau_d)v] + k_2\Delta v \quad (13)$$

③ IDM for HDV

The improved IDM Car-following model expression is as follows:

$$a_h = \lambda_n a_{\max} \left\{ 1 - \left( \frac{v}{v_f} \right)^4 - \left[ \frac{s_h + v(\omega_n t_h + \tau_h) + v\Delta v(2\sqrt{a_{\max} b})^{-1}}{x_h - l} \right]^2 \right\} \quad (14)$$

where:  $\tau_c, \tau_d, \tau_h$  are the reaction times of the CAV, the DCAV, and HDV respectively, and are taken as 0 s, 0.2 s, 0.4 s.

### 3.3. Validation of Mixed Traffic Flow Following the Model

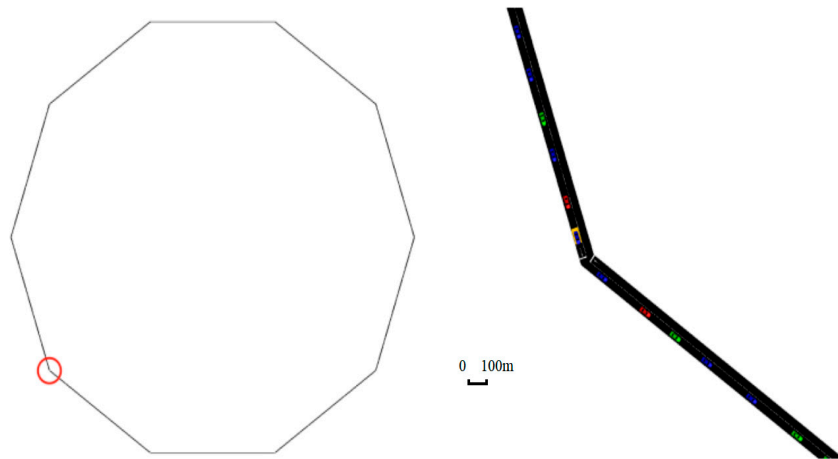
To test the scientific validity of the mixed traffic flow following the model established in the previous paper, simulation experiments are designed, and the control variable method is used to test the influencing factors involved, respectively. When the simulated density-flow scatter plot is consistent with the theoretical density-flow curve, it is considered that the established car-following model has a certain degree of scientific validity and can describe the car-following characteristics of mixed traffic flow.

(1) Simulation scenario setup

The simulation scenario setup is described in six aspects: road section setup, speed setup, flow setup, simulation parameter setup, data detection setup, and data collection and processing.

① Road section setup: Since the length of the simulated road section is set to be about 10,000 m, because the first car must follow the speeding front car, the ring road network is selected, as shown in Figure 3, Figure 3b specifically zooms in on the area highlighted by the red circle in Figure 3a, providing a detailed view of the critical section.

② Speed setting: the maximum speed of the urban road section is set to 11.1 m/s. In order to get the flow density scattering when the density is large, the simulation is run for a certain period of time. The speed reduction interference is carried out on the last road section and the road first Section 1 to reduce the speed of the vehicles on its road section to 1 m/s.



(a) Traffic flow diagram simulation scene diagrams

(b) Traffic flow diagram part simulation scene diagram

**Figure 3.** Base map simulation road network diagram.

③ Traffic flow setting: firstly, define three types of vehicles, namely, “HDV”, “ACC”, and “CACC”, and set the parameters of the following model in the same way as the theoretical analysis in Sections 2.1 and 2.2; secondly, define the traffic flow of the three types of vehicles in order to obtain the mixed traffic flow with different penetration rates of CAVs and Fleet Composition. Secondly, define the traffic flow of the three types of vehicles to obtain the mixed traffic flow with different penetration rates of CAV and Fleet Composition.

④ Simulation parameter setting: the simulation duration is 18,000 s, and the simulation step size is 0.1 s.

⑤ Data detection setting: For the ten road sections set up in the simulation, data detection is performed on each road section with a frequency of 120 s. The detection frequency is 120 s (i.e., the speed, density, vehicle number, and other information of each section are counted every two minutes, and the flow rate is calculated from the statistical density and speed data).

⑥ Data Collection and Processing: Based on preliminary experimental predictions, after the simulation starts running for 60 s, the simulation state becomes stable. Data is collected every 120 s thereafter. Speed and flow information is recorded using edge detectors, and density data is collected using spot detectors. The collected data includes the average speed (the average speed of all vehicles in each road section), the average density (the average number of vehicles per kilometer per lane in each road section), and the flow (vehicles per hour). In this study, data collection lasted for 18,000 s (five hours, with a total of 150 data collection instances). Data was collected every 120 s, and each collection included 150 times, 10 road sections, and each road section had 1500 data points.

First, Python scripts were used to define the parameters (such as length, width, limits, and expected speeds) of different vehicle types and routes in the traffic flow file using <routes>. Then, Python scripts were used to set the car-following model parameters for each vehicle type. Among them, the car-following model function for CAV is given by Equation (11) in Section 2.2. The degraded car-following model function for DCAV is given by Equation (12), while the car-following model function for HDV is provided by Equation (13) and each vehicle type’s acceleration was updated to match the corresponding car-following model parameters (using a self-developed automated speed update algorithm). Simultaneously, the traffic flow file, route file, and corresponding attachment files were called to perform the simulation.

## (2) Analysis of Simulation Results

According to the results of the simulation output of the penetration rate, reaction time, and safety headway sensitivity coefficient of CAV, and combined with their corresponding theoretical curves, the following visualization is made, in which the red curve is the



theoretical curve, and the blue scatter points are the flow density points obtained in the simulation (the anomalous points are mainly generated due to the speed reduction interference on some road sections, and when comparing the flow density scatter points obtained by the simulation and the theoretical curve, they can be ignored) (The anomalies are mainly due to the speed reduction interference on some road sections and can be ignored when comparing the flow density scatter points obtained from the simulation and the theoretical curve).

#### Penetration Rate of CAV

To verify the correctness of the mixed traffic flow following model after the introduction of the penetration rate of CAV, the reaction time  $\tau = 0.4$  s, the sensitivity coefficient of safe headway  $\omega_n = 1.30$ , and its penetration rate of CAV  $P_1$  are taken as 0, 20%, 40%, 60%, 80%, and 100%, respectively, and the simulation results are shown in Figure 4.

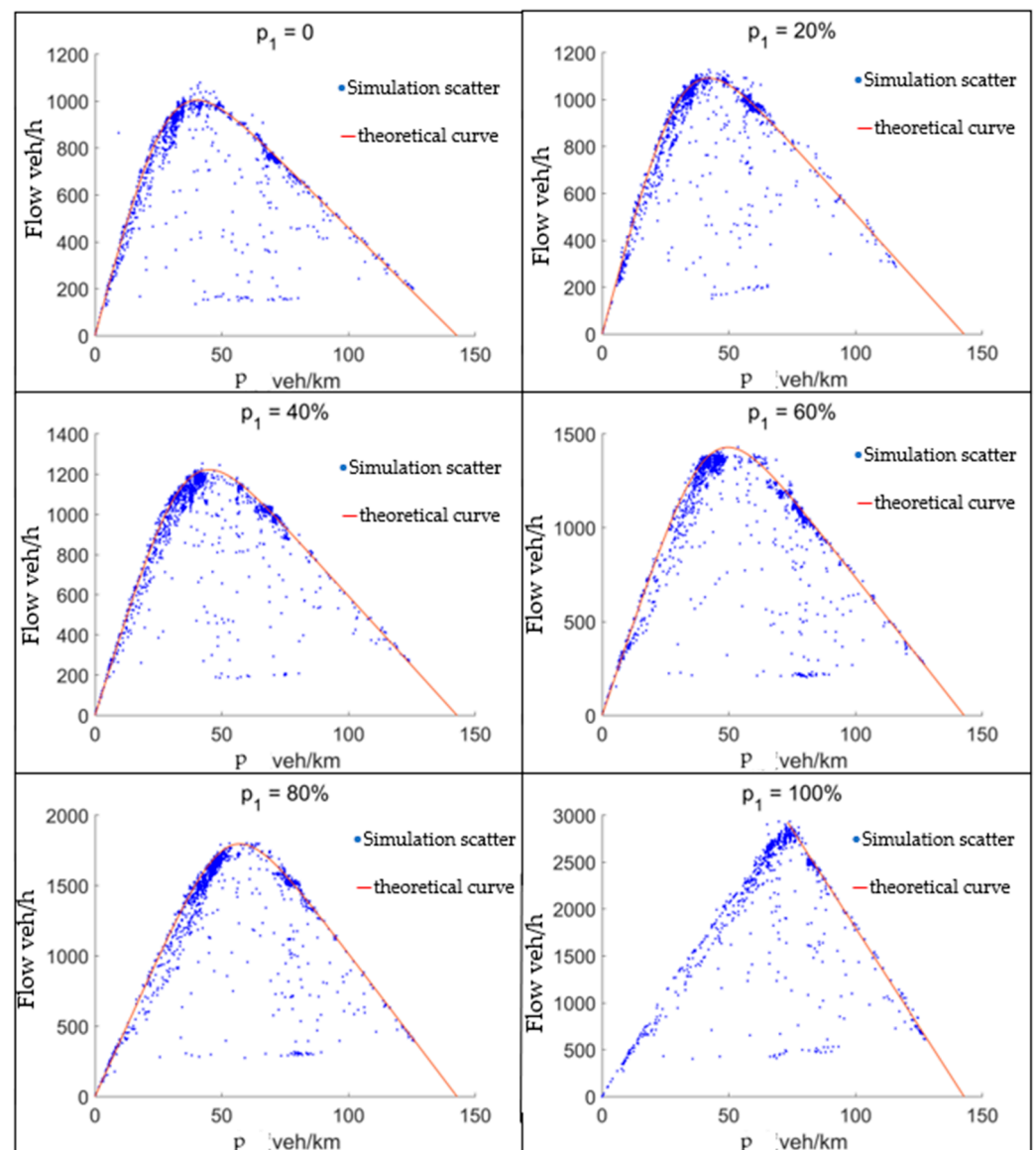


**Figure 4.** Simulated scatter versus theoretical curves at different penetration rates.

From the above figure, the maximum flow rate obtained from the simulation increases with the increase in the penetration rate of the CAV if the other parameters are constant and most of the scatter points are distributed on both sides of the theoretical curve.

#### Response Time (Technology)

In order to verify the correctness of the mixed traffic flow following model after the introduction of reaction time, so that the penetration rate of CAV  $P_1 = 0$ , the safety headway sensitivity coefficient  $\omega_n = 1.30$ , and its reaction time  $\tau$  are taken as 0.3 s, 0.5 s, 0.6 s, and 0.7 s, respectively, and the simulation results are shown in Figure 5.

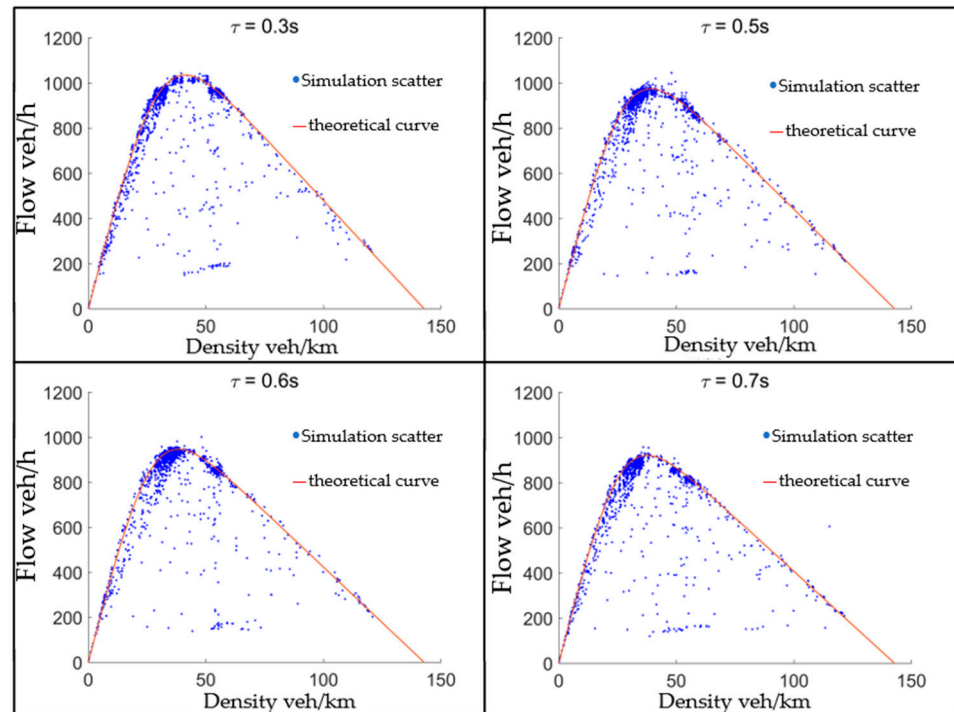


**Figure 5.** Simulated scatter versus theoretical plots for different reaction times.

From the above figure, the maximum flow rate obtained from the simulation decreases as the reaction time increases, and most of the scatter points are distributed on both sides of the theoretical curve when the other parameters are constant.

#### Safe Flow Sensitivity Factor

To verify the correctness of the mixed traffic flow following model after the introduction of the safety headway sensitivity coefficient, the penetration rate of the CAV  $P_1 = 0$ , the reaction time  $\tau = 0.4$ , and its safety headway sensitivity coefficient  $\omega_n$  are taken as 0.65 and 1.91, respectively, and the simulation results are shown in Figure 6.

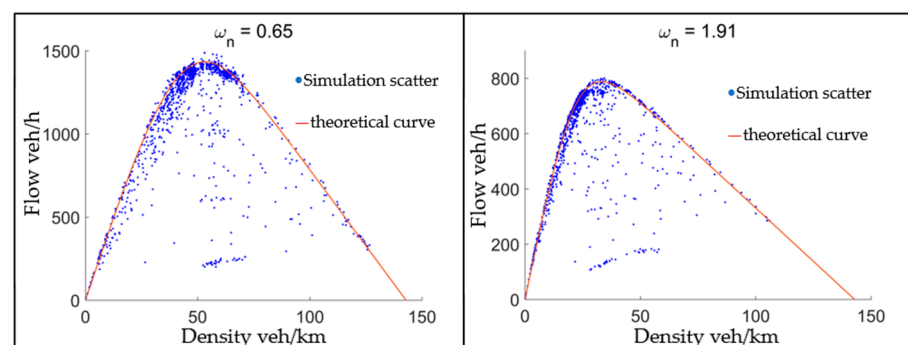


**Figure 6.** Simulation scatter versus theoretical curves with different safety headway P.

#### Sensitivity Coefficients

From the above figure, the maximum flow rate obtained from the simulation decreases with the increase of the safety headway sensitivity coefficient at constant values of the other parameters, and most of the scatter points are distributed on both sides of the theoretical curve.

In summary, the flow density scatter points obtained from the simulation are in high agreement with the theoretical curves, thus verifying the scientific validity of the previous paper in establishing a mixed traffic flow following model based on the following characteristics and reaction time.

#### 4. Characterization of Mixed Traffic Flow Considering Fleet Composition

##### 4.1. Basic Diagram Model Based on Fleet Composition

When the traffic flow is in equilibrium, the acceleration of the vehicles and the speed difference between them are 0. Therefore, the acceleration and speed difference in Equations (11)–(13) are set to be 0 to obtain the headway of the CAV, the degraded CAV, and the HDV in equilibrium, respectively, as shown in the following equation:

$$x_c = s_c + l + (t_c + \tau_c)v \quad (15)$$

$$x_d = s_d + l + (t_d + \tau_d)v \quad (16)$$

$$x_h = \frac{s_h + v(\omega_n t_h + \tau_h)}{\sqrt{1 - (v/v_f)^4}} + l \quad (17)$$

Assuming that the length of the roadway covered by the mixed traffic flow with  $N$  vehicles is  $L$  (unit m), which is the sum of the headway spacing of all vehicles, at this point, combining Equations (1)–(5) and Table 1, the length of the mixed traffic flow is shown in the following equation when the penetration rate of CAV and the Fleet Composition are  $p_1$  and  $O$ , respectively:

$$L = N\{p_1 p_{11}(p_1, O)x_c + p_1 p_{10}(p_1, O)x_d + p_0 x_h\} \quad (18)$$

Based on the relationship between the traffic flow density and the length of road coverage, the following expression is obtained:

$$k = \frac{1000}{p_1 p_{11}(p_1, O)x_c + p_1 p_{10}(p_1, O)x_d + p_0 x_h} \quad (19)$$

where:  $k$  is the traffic flow density in units of veh/km.

Substituting Equations (15)–(17) into Equation (19), we obtain the density-velocity relationship as follows:

$$k = 1000 \left\{ \begin{array}{l} p_1 p_{11}(p_1, O)[s_c + l + (t_c + \tau_c)v] \\ + p_1 p_{10}(p_1, O)[s_d + l + (t_d + \tau_d)v] + p_0 \left[ \frac{s_h + v(\omega_n t_h + \tau_h)}{\sqrt{1 - (v/v_f)^4}} + l \right] \end{array} \right\}^{-1} \quad (20)$$

The macroscopic traffic flow relationship between flow, density, and velocity is  $q = kv$  (veh/h), which leads to the following flow-velocity relationship:

$$q = 3600v \left\{ \begin{array}{l} p_1 p_{11}(p_1, O)[s_c + l + (t_c + \tau_c)v] \\ + p_1 p_{10}(p_1, O)[s_d + l + (t_d + \tau_d)v] + p_0 \left[ \frac{s_h + v(\omega_n t_h + \tau_h)}{\sqrt{1 - (v/v_f)^4}} + l \right] \end{array} \right\}^{-1} \quad (21)$$

Analyzing Equations (20) and (21), it can be seen that the relational equations between flow-density-speed are all affected by (i) the reaction time of the vehicle, which is manifested in the compensation of the front-end time distance; (ii) the degradation of the CAV, which is manifested in the classification of the vehicle types and different following models; and (iii) the Fleet Composition, which is manifested in the determination of the probability of the emergence of different following models for a certain penetration rate of the CAV; (iv) human driver characteristics, which is manifested in categorizing human driver styles

when the HDV is used as a following vehicle. This study considers the impact of human drivers' uncertainty on mixed traffic flow when facing CAV, which is closer to the actual situation of mixed traffic flow on urban roads compared to other studies.

Let the Fleet Composition  $O = 0$ , when the HDV is used as a following vehicle, let the driver be a smooth type, i.e., the safety headway sensitivity coefficient  $\omega_n = 1.30$ , and according to Equations (20) and (21) the basic diagrams can be obtained as shown in Figures 7–9 with different penetration rates of the CAV:

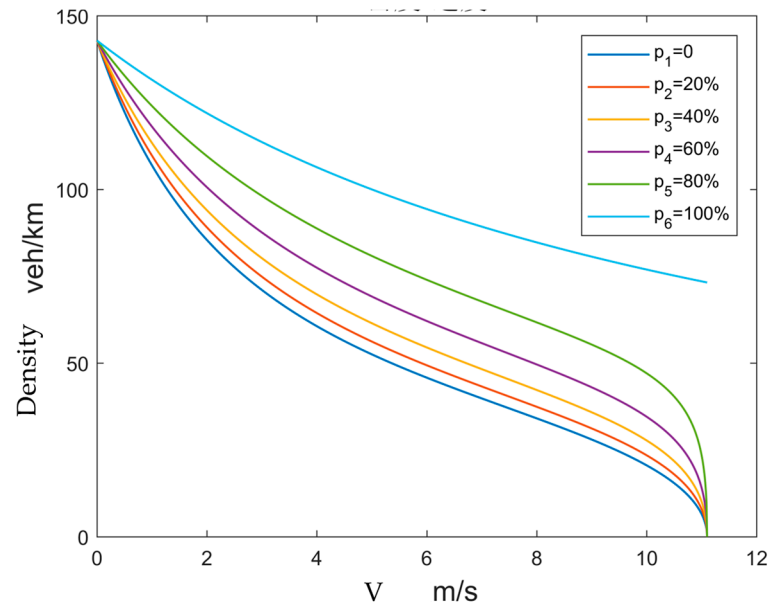


Figure 7. Flow-velocity diagram.

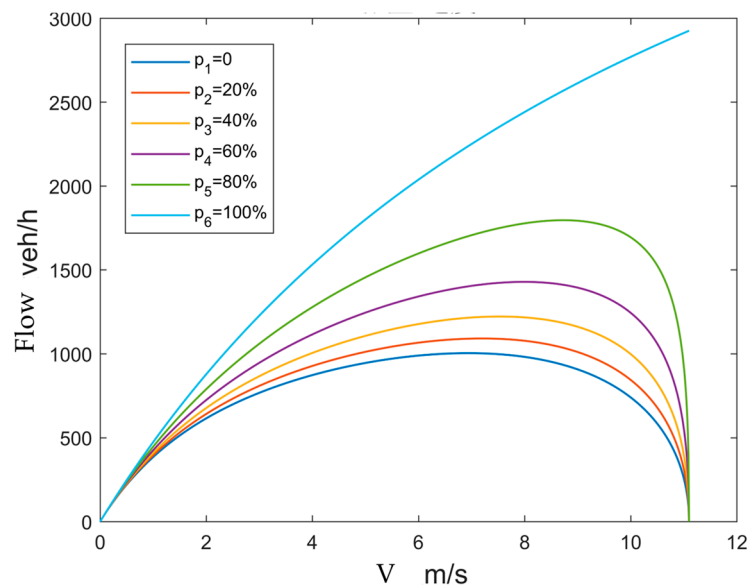


Figure 8. Density-velocity diagram.

Analyzing the above three figures, increasing the penetration rate of CAV helps to improve the capacity of mixed traffic flow on urban roads when other influencing factors are certain. As shown in Table 5, as the penetration rate of CAV increases, the optimal density of the traffic flow and its corresponding critical speed gradually increase, and the flow rate is the largest when the penetration rate of CAV is the largest, at which time there are only CAV in the traffic flow, corresponding to the optimal density of the traffic flow of 73.21 veh/km, and the maximum flow rate is 2925 veh/h, which is about 2.91 times of the

capacity of the traditional HDV. Therefore, the inclusion of CAV plays a positive role in improving the congestion problem on urban roads.

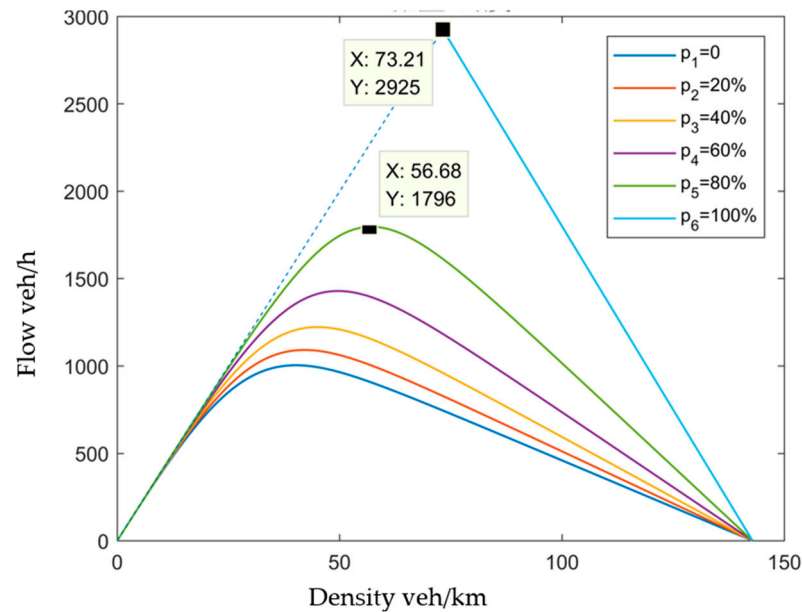


Figure 9. Flow-density diagram.

Table 5. Values of the sensitivity coefficients  $\lambda_n$ ,  $\omega_n$  and the style of Car-following.

CACC Penetration Rates $p/\%$	Maximum Flow Rate (veh/h)	Optimal Density (veh/km)	Critical Velocity (km/h)
0	1004	40.60	25.34
20	1091	43.01	26.50
40	1222	45.86	27.61
60	1429	49.67	28.87
80	1796	56.83	31.78
100	2925	73.21	40.00

#### 4.2. Parameter Sensitivity Analysis

In order to further investigate the effects of reaction time  $\tau$ , Fleet Composition  $O$ , and driver following characteristics  $\omega$  when the HDV is the rear vehicle on the mobility of mixed traffic flow on urban roads in the basic diagram model, the flow density change diagrams were analyzed by the control variable method when the influencing parameters took different values, respectively.

##### (1) Reaction time $\tau$ sensitivity analysis

The reaction time required for sending and receiving information between CAV in the mixed traffic flow is determined, while the reaction time of HDV is uncertain due to the involvement of human drivers, so that the Fleet Composition  $O = 0$  and the safe headway sensitivity coefficient  $\omega_n = 1.30$ , and the reaction time  $\tau$  in the basic diagram are taken as 0.3 s, 0.4 s, 0.5 s, 0.6 s, and 0.7 s, respectively, and the flow density diagram can be obtained as shown in Figure 10:

$\tau = 0.4$  s when it is shown in Figure 10. When the penetration rate of CAV is 100%, i.e., there are no HDV on the whole road, which is not affected by the reaction time, the following table shows the maximum flow rate  $Q_m$  corresponding to different reaction times  $\tau$  when the penetration rate of CAV is 0%, 20%, 40%, 60%, and 80%.

Combined with Figure 10 and Tables 2–6, the longer the reaction time of the HDV, its optimal density and maximum flow of traffic flow gradually decrease, so the road capacity decreases; therefore, the reaction time will have a negative effect on the road capacity.



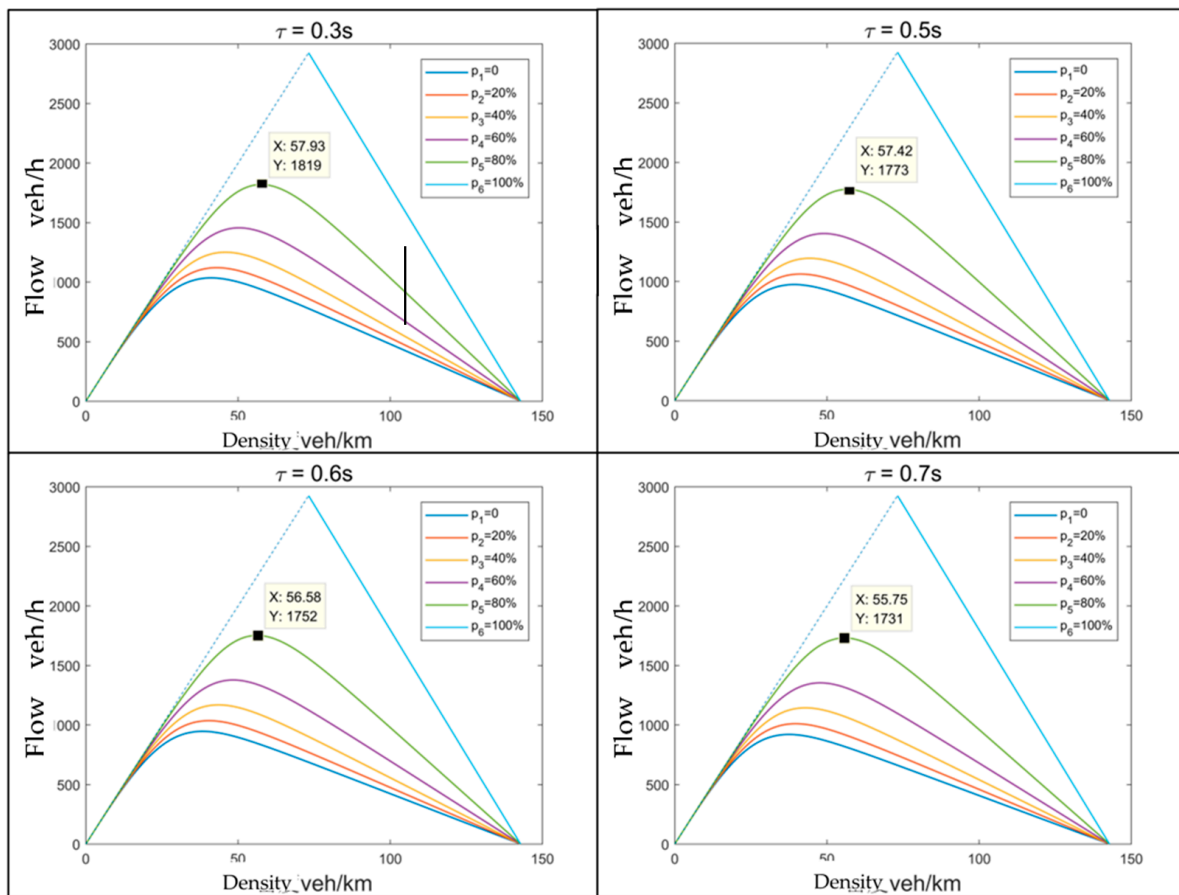


Figure 10. Effect of reaction time on maximum flow and optimal density of mixed traffic flow.

Table 6. Different reaction times  $\tau$  and maximum flow rate  $Q_m$ .

Response Time (Technology) $\tau/s$	$p_1 = 0$	$p_1 = 0.2$	$p_1 = 0.4$	$p_1 = 0.6$	$p_1 = 0.8$
	Maximum Flow Rate $Q_m$ (/veh/h)				
0.3	1035	1121	1251	1456	1819
0.4	1004	1091	1222	1429	1796
0.5	974	1063	1195	1403	1773
0.6	946	1036	1169	1378	1752
0.7	920	1010	1144	1354	1731

(2) Fleet Composition  $O$  Sensitivity Analysis

Fleet Composition is an important parameter to study the fleet characteristics of mixed traffic flow, so that the basic diagram of the HDV reaction time  $\tau = 0.4$  and safety headway sensitivity coefficient  $\omega_n = 1.30$ , Fleet Composition  $O$  are obtained as  $-1, -0.5, 0, 0.5, 1$ , respectively, when the flow density diagram shown in Figure 11:

$O = 0$  as is shown in Figure 11. When the penetration rate of CAV is between 100% and 0%, the traffic flow is homogeneous and is not affected by the Fleet Composition, so the following table shows the maximum traffic flow  $Q_m$  corresponding to different Fleet Composition  $O$  when the penetration rate of CAV is between 20%, 40%, 60%, and 80%.

Combined with Figure 11 and Table 7, it can be seen that when the penetration rate of CAV  $p_1 = [0.2, 0.8]$ , the optimal density and maximum flow rate of traffic flow increase with the increase of Fleet Composition, and the road capacity increases significantly, so the improvement of Fleet Composition is conducive to the improvement of road capacity.

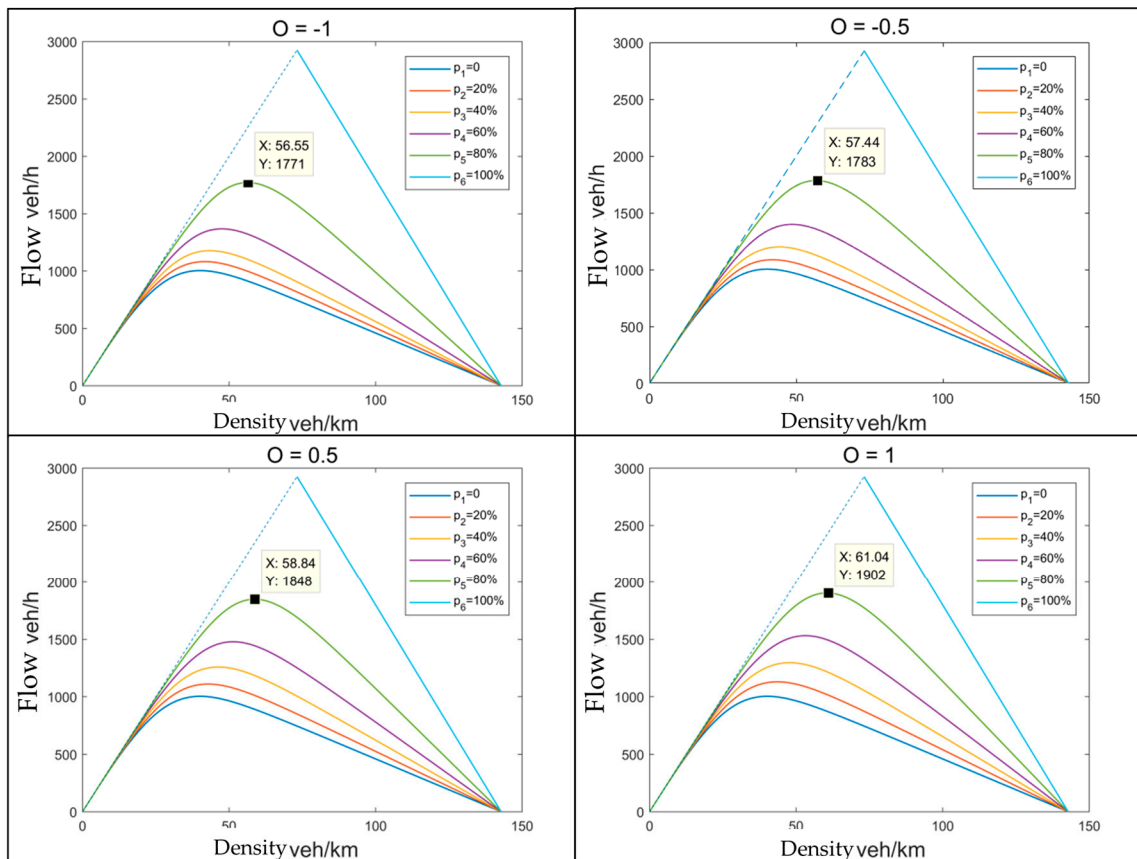


Figure 11. Effect of Fleet Composition on maximum flow and optimal density of mixed traffic flow.

Table 7. Different Fleet Compositions  $O$  and maximum flows  $Q_m$ .

Vehicle Strength $O$	$p_1 = 0.2$	$p_2 = 0.4$	$p_3 = 0.6$	$p_4 = 0.8$
	Maximum Flow Rate $Q_m$ (/veh/h)			
-1	1082	1177	1368	1771
-0.5	1087	1199	1397	1784
0	1091	1222	1429	1796
0.5	1110	1258	1478	1848
1	1129	1296	1531	1902

(3) Driver Following Characteristics when HDV as Rear Vehicle  $\omega$  Sensitivity Analysis

Considering that human drivers have different degrees of acceptance of CAV, they will have different driver following characteristics when following CAV, so that when the reaction times of the HDV  $\tau = 0.4$  and the Fleet Composition  $O = 0$ ,  $\omega_n$  in the basic graph are taken as 0.65, 1.30, and 1.91, respectively, the traffic density diagram can be obtained as shown in Figure 12:

$\omega_n = 1.31$  as is shown in Figure 12. When the penetration rate of CAV is 100%, there is no HDV in the traffic flow, so the following table shows the maximum flow rate  $Q_m$  corresponding to the safe headway sensitivity factor  $\omega_n$  when the penetration rate of CAV is 0%, 20%, 40%, 60%, and 80%.

Combined with Figure 12 and Table 8, it can be seen that in the presence of a HDV in the traffic flow, the optimal density and maximum flow rate of the traffic flow decrease with the increase of the safety headway sensitivity coefficient, and the road capacity decreases significantly; therefore, when the human driver’s trust in the intelligent network is of the hesitant type, it will have a negative effect on the road capacity, and when the

human driver’s trust in the intelligent network is of the trusting type, it is beneficial to the improvement of the road capacity.

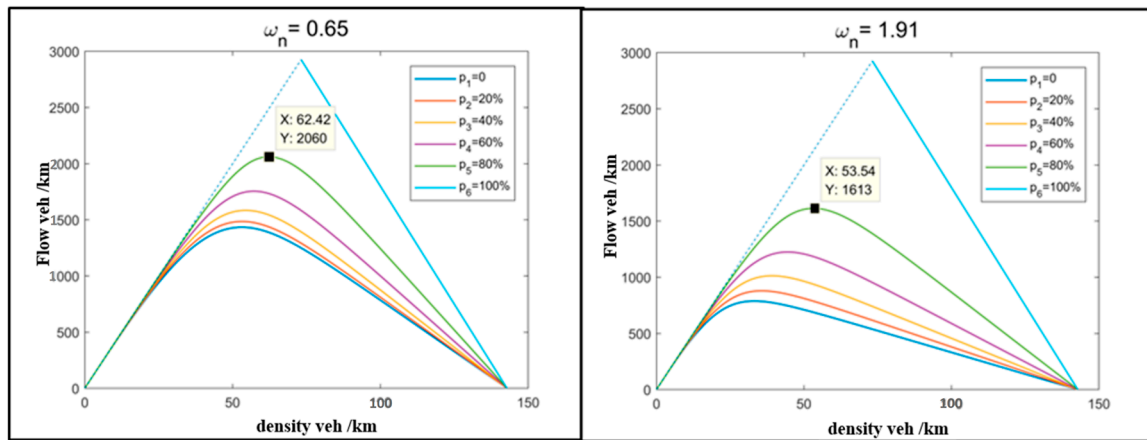


Figure 12. Effect of Fleet Composition on maximum flow and the optimal density of mixed traffic flow.

Table 8. Sensitivity coefficients for different safety headway hourly distances  $\omega_n$  and maximum flow rate  $Q_m$ .

Safe Headway Time Sensitivity Factor $\omega_n$	$p_1 = 0$	$p_2 = 0.2$	$p_3 = 0.4$	$p_4 = 0.6$	$p_5 = 0.8$
	Maximum Flow Rate $Q_m$ (/veh/h)				
0.65	1433	1485	1583	1754	2060
1.30	1004	1091	1222	1429	1796
1.91	787	878	1012	1224	1613

(4) A comprehensive analysis of multiple influencing factors

Figures 13–15 show the variation of the capacity of each influencing factor at different penetration rates of CAV, respectively.

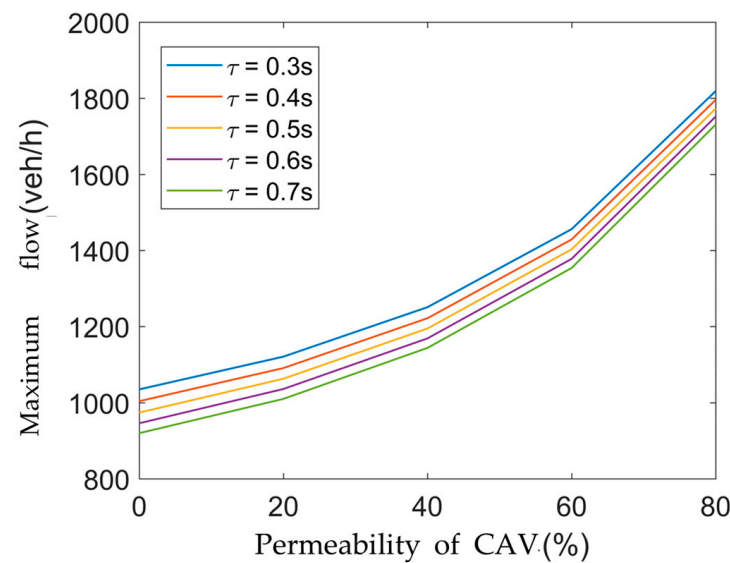


Figure 13. Different reaction times  $\tau$  and maximum flow rate  $Q_m$ .

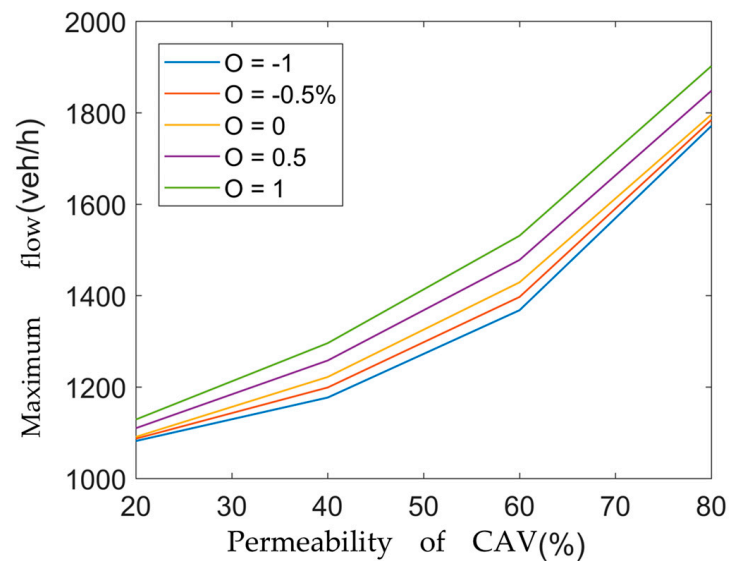


Figure 14. Varying Fleet Compositions  $O$  and maximum flows  $Q_m$ .

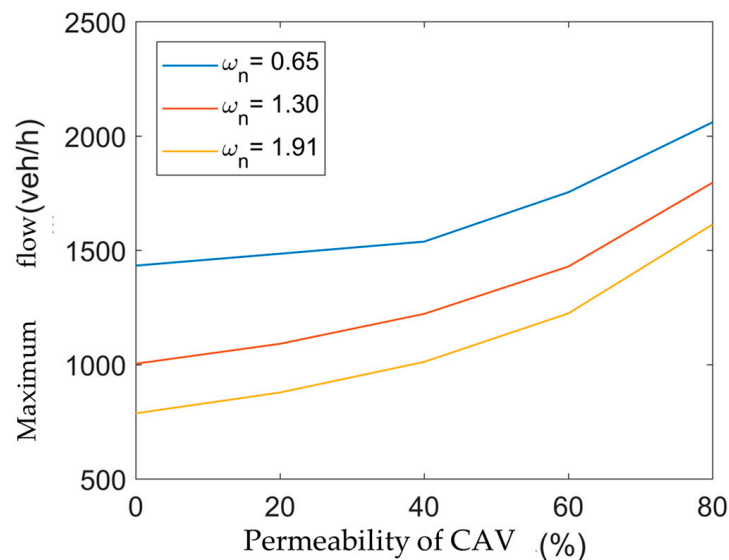
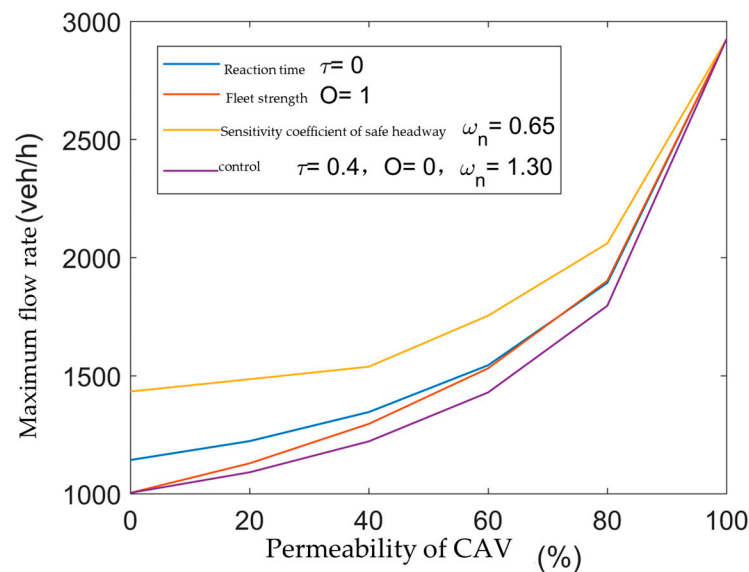


Figure 15. Sensitivity coefficients for different safety headway time distances  $\omega_n$  and maximum flow rates  $Q_m$ .

Through observation, when the reaction time, Fleet Composition, and safety headway sensitivity coefficient are certain, with the increase in the penetration rate of CAV, the road capacity gradually improves, and all of them show the trend that the growth rate of the second half is greater than that of the first half. It shows that: ① the increase of CAV can compensate for the negative effect of human drivers' reaction on road capacity; ② the increase of CAV can strengthen the effect of Fleet Composition on road capacity; ③ the increase of CAV can compensate for the adverse effect of hesitant human drivers on road capacity and strengthen the role of trustworthy human drivers to improve road capacity; ④ the increase of CAV can compensate for the adverse effect of hesitant human drivers on road capacity and strengthen the role of trustworthy human drivers to improve road capacity. (iv) The higher the penetration rate of CAV, the better the effect of compensation or reinforcement.

As can be seen in Figure 16, at reaction time  $\tau = 0$  or Fleet Composition  $O = 1$  or safety headway sensitivity factor  $\omega_n = 0.65$ , which correspond to the respective maximum flow rates, it is clear that optimizing all three influencing factors improves the road capacity when compared to the control group, as shown in Figure 13. When  $p_1$  is taken as 0%, 20%, 40%,

and 60%, the influence of each influencing factor on the road capacity is  $\omega > O > \tau$ , and when  $p_1$  is taken as 80%, the influence of the influencing factor  $\tau$  on road capacity exceeds that of the influence factor  $O$ , and the influencing factor  $\omega$  is always in the first place.



**Figure 16.** Maximum flow rate for each parameter in the ideal condition  $Q_m$ .

#### 4.3. Mixed Traffic Flow Characteristics at Intersections

On urban roads, continuous traffic flow is frequently interrupted by intersections. To analyze the characteristics of mixed traffic flow at intersections, a simulation experiment was designed to compare the number of stops and delays, assessing the impact of CAV on traffic flow. The study scenario includes the following constraints:

- (1) The research scope is limited to a single intersection with fixed signal timing for through vehicles.
- (2) The effects of adjacent intersections, roadside parking, and pedestrians are not considered.
- (3) CAV can share real-time road traffic information.
- (4) The wireless communication performance between vehicles and between vehicles and traffic signals is reliable, with no delays or data loss in traffic information transmission.

##### 4.3.1. Experimental Setup

###### (1) Simulation Scenario Construction

**Road Network:** Utilizing the “netedit” tool, a city road network with a two-lane intersection was created. The road lengths for the east, south, west, and north approaches to the intersection were set to 300 m, 50 m, 50 m, and 50 m, respectively, with traffic signals installed at the intersection.

**Vehicle Definition and Generation:** Three types of vehicles were defined: CAV, Degraded Connected and Autonomous Vehicles (DCAV), and HDV, each with a length of 5 m. At the beginning of the simulation, the generation probabilities of CAV and HDV were controlled to obtain traffic flows with different CAV penetration rates, ensuring a random distribution of CAV and HDV.

**Simulation Process:** The simulation step length was set to 1, updating vehicle positions and speeds within each time step.

###### (2) Traffic Parameter Settings

**Road Parameters:** The maximum speed for all roads in the simulation was set to 11.1 m/s, with each lane width set to 3.5 m, the standard width for urban roads. To simulate realistic conditions at urban road intersections, white solid lines were placed within 60 m of the intersection to prohibit lane changes in this area.



Vehicle Behavior Model: Vehicles entered the road at random speeds with their departure positions set to zero. The car-following model used was the mixed traffic flow car-following model established in Section 2.2, while the lane-changing model employed was the Krauss model.

Traffic Signal Configuration: Traffic signals in the simulation had fixed phases, with red light time, all-red time, green light time, and yellow light time set to 14 s, 3 s, 30 s, and 3 s, respectively. The simulation scenario is depicted as illustrated in Figure 17.



Figure 17. Intersection Simulation Scenario Diagram.

#### 4.3.2. Experimental Results Analysis

To evaluate the impact of CAVs on traffic flow at intersections, a two-lane intersection was set up with a flow rate of 1800 vehicles per hour. The penetration rate of CAVs in the mixed traffic flow was varied at 20%, 40%, 60%, and 80%. To eliminate random errors, 20 experiments were conducted for each CAV penetration rate condition, with data from 100 vehicles collected continuously in each experiment. The results of these experiments were then analyzed. The data is organized as illustrated in Table 9.

Table 9. Number of Stops and Delays in Mixed Traffic Flow at the Intersection with Different CAV penetration rates.

Number of Experiments	Penetration Rates of CAV							
	20%		40%		60%		80%	
	Delay (s)	Stop (Times)	Delay (s)	Stop (Times)	Delay (s)	Stop (Times)	Delay (s)	Stop (Times)
1	355	69	385	58	484	59	281	43
2	645	82	452	68	406	62	397	52
3	481	84	483	85	464	63	577	59
4	518	89	523	82	469	60	419	52
5	468	69	371	58	337	54	353	58
6	423	58	457	72	395	55	360	51
7	401	78	372	68	476	65	337	46
8	453	67	452	68	383	49	452	55
9	469	95	355	68	297	53	477	58
10	520	86	477	75	478	57	423	51
11	314	65	523	77	521	61	294	45
12	609	91	370	63	538	56	402	52
13	522	84	380	63	408	61	434	50
14	497	76	325	63	326	56	381	52
15	558	81	383	72	363	51	383	50
16	524	81	476	73	525	69	470	56
17	559	69	470	65	331	59	472	56
18	551	75	394	67	313	64	552	62
19	556	91	413	83	389	51	350	47

Table 9. Cont.

Number of Experiments	Penetration Rates of CAV							
	20%		40%		60%		80%	
	Delay (s)	Stop (Times)	Delay (s)	Stop (Times)	Delay (s)	Stop (Times)	Delay (s)	Stop (Times)
20	486	96	486	72	383	58	348	46
Average	495.4	79.3	427.3	70.0	414.3	58.1	408.1	52.0
Average Delay	4.954	0.793	4.273	0.70	4.143	0.581	4.081	0.52

The table shows that the average delay times for CAV penetration rates of 20%, 40%, 60%, and 80% are 4.954 s, 4.273 s, 4.143 s, and 4.081 s, respectively, and the average number of stops is 0.793, 0.700, 0.581, and 0.520, respectively. As the penetration rates of CAVs increase, both the average delay time and the average number of stops gradually decrease.

The space-time trajectory diagram visualizes the movement trajectories of vehicles in time and space, describing the changes in vehicle positions over time during the simulation. The horizontal and vertical axes represent time and position, respectively. In this study, the blue and orange curves in the space-time trajectory diagram represent vehicles in two adjacent lanes, respectively. Vehicles entered the road at random speeds, and a data set closest to the average number of stops was selected for the space-time trajectory diagram. The simulation results are depicted as shown in Figure 18.

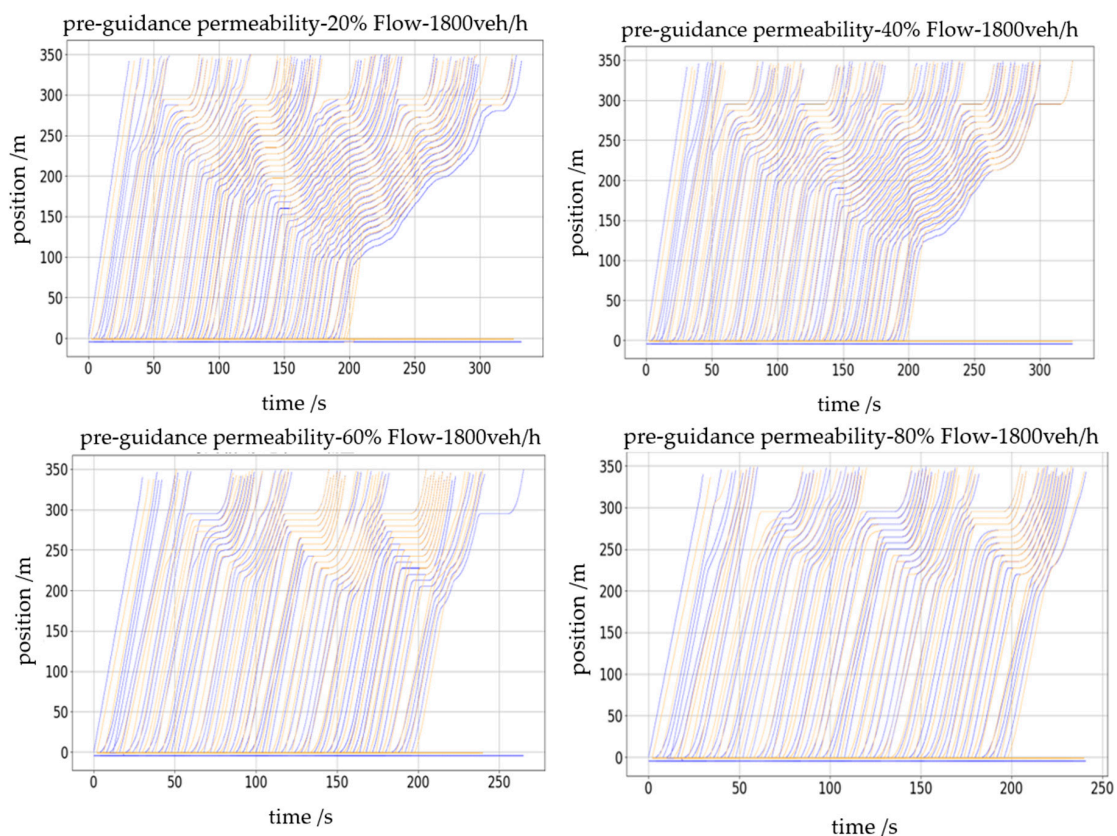


Figure 18. Space-Time Trajectories at the Intersection for Different CAV penetration rates.

Comparing the space-time trajectory diagrams for different CAV penetration rates, the fluctuations in trajectories significantly decrease as the penetration rates of CAV increase, and the number of stops at intersections noticeably reduces. This is likely because CAV can promptly obtain signal control information at intersections and communicate with each other. Consequently, CAVs can adjust their speeds to minimize stopping at inter-

sections. As the penetration rates of CAV increase, they gradually dominate the mixed traffic flow, indirectly influencing HDV and making the entire mixed traffic flow smoother at intersections.

## 5. Conclusions

In this study, firstly, we classified the possible following situations in the mixed traffic flow of urban roads and constructed the mathematical analytical expressions of the stochastic distribution characteristics of different types of vehicles. Secondly, a mixed traffic flow following model is established by considering the early stages of connected automated vehicle (CAV) deployment, where there is uncertainty regarding the acceptance and trust levels of human drivers. The car-following behavior of manually driven vehicles behind CAVs is categorized into three styles: hesitant, stable, and trusting. Subsequently, a fundamental diagram model considering Fleet Composition was derived, and the characteristics of mixed traffic flow at intersections were analyzed. The main conclusions are as follows:

- (1) Reaction time adversely affects road capacity. As the reaction time increases, the optimal density and maximum flow rate of the traffic flow gradually decrease, and the road capacity decreases.
- (2) As the concentration of CAV increases, the optimal density and maximum flow rate of the traffic stream gradually increase, enhancing the road capacity.
- (3) The safe headway sensitivity coefficient of human drivers has a negative effect on road capacity. As the safe headway sensitivity coefficient increases, the optimal density and maximum flow rate of traffic flow gradually decrease, and the road capacity decreases significantly.
- (4) The degree of influence of each influencing factor on road capacity is roughly following: Fleet Composition > reaction time, with reaction time influencing road capacity more than Fleet Composition at a penetration rate of 80% of the CAV, and the human driver's style of following the CAV always ranks first in terms of its influence on road capacity. Our analysis rests on carefully considered assumptions, yet we humbly acknowledge the dynamic and unpredictable nature of technological progress. Future research must embrace this uncertainty, continually reassessing the influence of connected and autonomous vehicles as they evolve, to ensure our understanding aligns with the realities of tomorrow's transportation landscape.
- (5) The increase in the penetration rates of CAV reduces the number of stops and delay times of mixed traffic flow at intersections, making traffic flow smoother. This paper conducts a series of analyses on mixed traffic flow; however, the actual urban road traffic environment is more complex. Intersection control strategies, roadside parking, non-motorized vehicles, and pedestrians all cause varying degrees of interference with the traffic flow. Additionally, wireless communication delays can affect the information transmission efficiency of CAV. Future research will focus on a more in-depth exploration of these uncertainties.

**Author Contributions:** Conceptualization, H.L.; methodology, H.L.; software, K.N.; validation, K.N. and H.W.; formal analysis, H.W. and Z.W.; investigation, A.S.; resources, A.S. and Z.W.; data curation, A.S. and Z.W.; writing—original draft preparation, K.N.; writing—review and editing, H.W.; visualization, H.W.; supervision, H.L.; project administration, H.L.; funding acquisition, H.L. All authors have read and agreed to the published version of the manuscript.

**Funding:** This research was funded by the Science and Technology Research Project of Higher Education Institutions in Hebei Province, grant number QN2020151. The aim was to investigate the economic performance optimization of autonomous vehicles under platooning mode. We would like to express our gratitude to Shijiazhuang Tiedao University for providing the research infrastructure and technical support.

**Data Availability Statement:** Data are contained within the article.

**Conflicts of Interest:** The authors declare no conflicts of interest.

## References

1. Hua, X.; Wang, W.; Wang, H. Mixed traffic flow model for on-ramp system considering the influence of adaptive cruising vehicles. *J. Phys.* **2016**, *65*, 223–235.
2. Qin, Y.; Li, S. String Stability Analysis of Mixed CACC Vehicular Flow with Vehicle-to-Vehicle Communication. *IEEE Access* **2020**, *8*, 174132–174141. [[CrossRef](#)]
3. Cao, Z.; Lu, L.; Chen, C.; Chen, X. Modeling and Simulating Urban Traffic Flow Mixed with Regular and Connected Vehicles. *IEEE Access* **2021**, *99*, 10392–10399. [[CrossRef](#)]
4. Jiang, Y.; Hu, R.; Yao, Z.; Wu, P.; Luo, X. Analysis of stability and safety of heterogeneous traffic flow in intelligent networked vehicle environment. *J. Beijing Jiaotong Univ.* **2020**, *44*, 27–33.
5. Cui, Z.; Wang, X.; Ci, Y.; Yang, C.; Yao, J. Modeling and analysis of car-following models incorporating multiple lead vehicles and acceleration information in heterogeneous traffic flow. *Phys. A Stat. Mech. Its Appl.* **2023**, *630*, 129259. [[CrossRef](#)]
6. Lin, H.; Fang, H.; Wu, D. Mixed traffic flow model for CACC vehicles based on dynamic safety distance. *J. Beijing Jiaotong Univ.* **2022**, *46*, 36–42+51.
7. Zhang, J.; Hu, S. Continuous type metacellular automata traffic flow model with mixed CACC and ACC vehicles. *Sci. Technol. Eng.* **2022**, *22*, 6340–6346.
8. Ma, X.; Ge, H.; Cheng, R. Influences of acceleration with memory on stability of traffic flow and vehicle's fuel consumption. *Phys. A Stat. Mech. Its Appl.* **2019**, *525*, 143–154. [[CrossRef](#)]
9. Zong, F.; Shi, P.; Wang, M.; He, Z. Mixed flow following model for networked autonomous vehicles considering front and rear multi-vehicles. *Chin. J. Highw.* **2021**, *34*, 105–117.
10. Qin, Y.; Wang, H.; Wang, W. LWR model for Mixed Traffic Flow in smart grid environment. *China J. Highw.* **2018**, *31*, 147–156.
11. Xu, T.-J.; Yao, Z.-H.; Jiang, Y.-S.; Yang, T. A basic graph model considering the effect of reaction time in intelligent networked vehicle environment. *Highw. Transp. Sci. Technol.* **2020**, *37*, 108–117.
12. Chang, X.; Li, H.-S.; Rong, J.; Qin, L.-Q.; Yang, Y.-F. Analysis of traffic flow basic diagram model with mixed intelligent networked fleet. *J. Southeast Univ. Nat. Sci. Ed.* **2020**, *50*, 7.
13. Ma, Q.; Fu, B.; Zeng, H. Basic graph and stability analysis of heterogeneous traffic flow in smart grid environment. *Transp. Inf. Saf.* **2021**, *39*, 76–84.
14. Yao, Z.; Wang, Y.; Liu, B.; Zhao, B.; Jiang, Y. Fuel consumption and transportation emissions evaluation of mixed traffic flow with connected automated vehicles and human-driven vehicles on expressway. *Energy* **2021**, *230*, 120766. [[CrossRef](#)]
15. Kamal, M.A.S.; Taguchi, S.; Yoshimura, T. Intersection Vehicle Cooperative Eco-Driving in the Context of Partially Connected Vehicle Environment. In Proceedings of the 2015 IEEE 18th International Conference on Intelligent Transportation Systems, Gran Canaria, Spain, 15–18 September 2015.
16. Yao, H.; Li, X. Decentralized control of connected automated vehicle trajectories in mixed traffic at an isolated signalized intersection. *Transp. Res. Part C Emerg. Technol.* **2020**, *121*, 102846. [[CrossRef](#)]
17. Ye, L.; Yamamoto, T. Evaluating the impact of connected and autonomous vehicles on traffic safety. *Phys. A Stat. Mech. Its Appl.* **2019**, *526*, 121009. [[CrossRef](#)]
18. Wang, J.; Peeta, S.; He, X. Multiclass traffic assignment model for mixed traffic flow of human-driven vehicles and connected and autonomous vehicles. *Transp. Res. Part B Methodol.* **2019**, *126*, 139–168. [[CrossRef](#)]
19. Yang, X.-J.; Jia, X.-H.; Zhang, S.-B. Mixed traffic flow characteristics considering dynamic characteristics of car queues. *J. Jilin Univ.* **2024**, 1–14. [[CrossRef](#)]
20. Wu, D.H.; Peng, R.; Lin, X.L. Mixing Characteristics of Heterogeneous Traffic Flow in Intelligent Network. *J. Southwest Jiaotong Univ.* **2022**, *57*, 761–768.
21. Chen, X.; Sun, J.; Ma, Z.; Sun, J.; Zheng, Z. Investigating the long-and short-term driving characteristics and incorporating them into car-following models. *Transp. Res. Part C Emerg. Technol.* **2020**, *117*, 102698. [[CrossRef](#)]
22. Soni, S.; Reddy, N.; Tsapi, A.; van Arem, B.; Farah, H. Behavioral adaptations of human drivers interacting with automated vehicles. *Transp. Res. Part F Traffic Psychol. Behav.* **2022**, *86*, 48–64. [[CrossRef](#)]
23. Ghiasi, A.; Hussain, O.; Qian, Z.; Li, X. A mixed Road Capacity analysis and lane management model for connected automated vehicles: A Markov chain method. *Transp. Res. Part B Methodol.* **2017**, *106*, 266–292. [[CrossRef](#)]
24. Milanés, V.; Shladover, S.E.; Spring, J.; Nowakowski, C.; Kawazoe, H.; Nakamura, M. Cooperative Adaptive Cruise Control in Real Traffic Situations. *IEEE Trans. Intell. Transp. Syst.* **2014**, *15*, 296–305. [[CrossRef](#)]
25. Treiber, M.; Hennecke, A.; Helbing, D. Congested traffic states in empirical observations and microscopic simulations. *Phys. Rev. E Stat. Phys. Plasmas Fluids Relat. Interdiscip. Top.* **2000**, *62*, 1805–1824. [[CrossRef](#)] [[PubMed](#)]
26. Regulations of the People's Republic of China on the Implementation of the Road Traffic Safety Law [EB/OL]. Available online: [https://china.findlaw.cn/fagui/p\\_1/388787.html](https://china.findlaw.cn/fagui/p_1/388787.html) (accessed on 10 May 2022).
27. Liu, B.-X.; Zhang, H.-Y.; Wang, M.; Wu, H.; Zong, F. Research on human driving behavior while following an autonomous vehicle: Empirical evidence and modeling. *J. Transp. Eng. Inf.* **2023**, *21*, 14–28. [[CrossRef](#)]

**Disclaimer/Publisher's Note:** The statements, opinions and data contained in all publications are solely those of the individual author(s) and contributor(s) and not of MDPI and/or the editor(s). MDPI and/or the editor(s) disclaim responsibility for any injury to people or property resulting from any ideas, methods, instructions or products referred to in the content.